NJC

COMMUNICATION

View Article Online
View Journal | View Issue

Cite this: *New J. Chem.*, 2024, **48**, 6557

Received 21st November 2023,
Accepted 17th March 2024

DOI: 10.1039/d3nj05363f

rsc.li/njc

A biocompatible Mn-decorated metal–organic cage with sustainable CO release†

Xiaomei Ning,[ab] Peilin Yin,[b] Lixia Zhang,[b] Feng Gao,*[a] Youfu Wang *[b] and Jinghui Yang *[c]

Carbon monoxide (CO) is an important gaseous transmitter with various pharmacological effects. However, it is a challenge to deliver the proper amount of CO to a specific location. The clinical application of the developed CO-releasing materials (CORMA) with ambiguous structures is difficult. Here, we utilize a metal–organic cage (MOC) with an atomically precise structure as a nanocarrier to bond Mn-based CO-releasing molecules. The obtained MOC-based CORMA are structurally stable and can release CO under light irradiation. Additionally, the *in vitro* and *in vivo* biological evaluation demonstrate the low toxicity and good biocompatibility of this MOC-based CORMA, which can effectively inhibit the survival of HeLa cells by light-triggered CO release.

1. Introduction

Due to its stronger affinity for hemoglobin than oxygen, CO – known as "the silent killer" – has previously been considered a toxic substance. In-depth research has provided evidence for CO to be an endogenous gas transporter that plays an essential role in physiological processes and multiple pathological conditions.[1,2] Furthermore, CO is reported to alleviate damage from injury, inflammation, and stress in multiple organs, and is regarded as a protective gas for clinical therapeutics.[3,4] CO is considered a double-edged sword just like Paracelsus originally expressed, "The Dose Makes the Poison". Most studies conducted so far in healthy volunteers suggest that blood carboxyhemoglobin (COHb) levels up to 10% showed no adverse events, and the proportion of COHb lower than 15% is, in the majority of cases, unable to elicit protection and beneficial outcomes, thus leading to the "biological threshold" of CO tolerance in humans to be 10–15%.[5,6] Due to this narrow threshold, researchers can favourably develop controlled methods for the required amount of CO release at a specific location.

Benefiting from the rapid development of nanotechnologies and the physiological effect of nanomaterials, various CORMA, especially for nanomaterials, have been developed for diverse biological applications, such as proteins, assembled polymeric nanostructures, nanoscale metal–organic frameworks, porous silica, inorganic nanocrystals, and nanocomposites.[7–11] These nanomaterials can indeed effectively load CO and release it under certain external stimuli, such as light, ultrasound, X-ray, magnetic field, and reactive oxygen species.[12–15] However, the complex and ambiguous structure of these CORMA (in terms of characteristics, such as size, composition, and surface chemistry) presents a formidable challenge in their potential clinical transformations.[16] Therefore, CORMA with well-defined chemical and spatial structures are urgently needed for consideration in long-term development goals.

Among precise nanoobjects, metal–organic cages (MOCs) constructed through coordination between metal clusters or ions and organic ligands have received widespread attention as a rising star. MOCs with precise and tailorable nanostructures at the atomic level exhibit fascinating properties and functions for diverse applications.[17,18] With their diversity, regulatability, porosity, modifiability, biocompatibility, and stability, MOCs can serve as precise nanoagents or nanocarriers in disease diagnosis and treatment based on precision medicine.[19,20] In fact, a variety of delicate MOC-based nanoagents or nanocarriers for different biological applications have been developed that demonstrate outstanding performances.[21–23]

Herein, we developed a light-triggered CORMA based on MOCs for the first time through post-synthetic modification (PSM) of a MOC *via* coordination with Mn-based CO-releasing molecules. As illustrated in Scheme 1, tetrahedral MOCs based on trinuclear pyramidal Zr_3O clusters and 2,2-bipyridine-5,5-dicarboxylic acid (H_2BPyDC) ligands were constructed under

[a] *School of Resources, Environment and Materials, Guangxi University, Nanning 530004, China. E-mail: gaofeng@gxu.edu.cn*
[b] *School of Chemistry and Chemical Engineering, Frontiers Science Center for Transformative Molecules, Shanghai Jiao Tong University, Shanghai 200240, China. E-mail: wyfown@sjtu.edu.cn*
[c] *Department of Organ Transplantation, Shanghai Changzheng Hospital, Naval Medical University, Shanghai, 200003, China. E-mail: yjh@smmu.edu.cn*

† Electronic supplementary information (ESI) available. See DOI: https://doi.org/10.1039/d3nj05363f

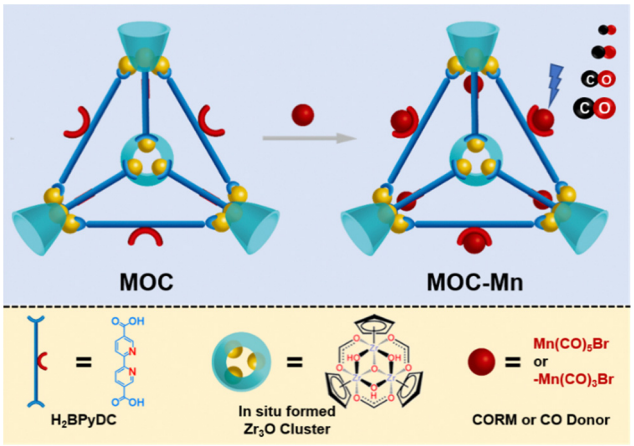

Scheme 1 The preparation, structure, and light-triggered CO release of MOC-Mn.

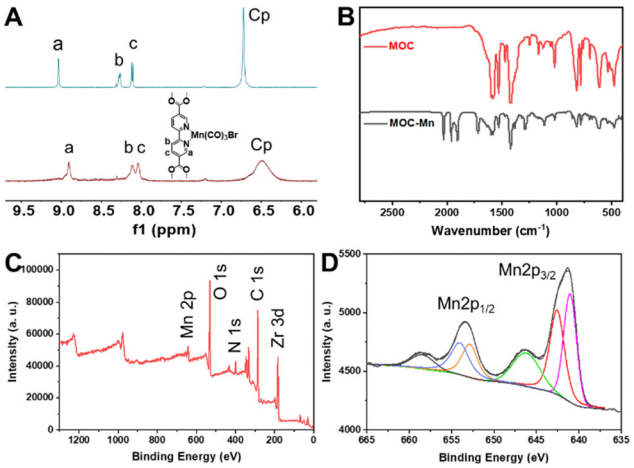

Fig. 1 The structural characteristics of MOC and MOC-Mn. (A) and (B) The ^{1}H-NMR and FTIR spectra of MOC (up) and MOC-Mn (bottom), respectively. (C) and (D) The full and high-resolution XPS spectra of MOC-Mn.

the solvothermal method. Accessible bipyridyl sites within the MOC were then coordinated with manganese pentacarbonyl bromide ($Mn(CO)_5Br$), a typical CO-releasing molecule, to obtain an MOC-based CORMA, named MOC-Mn. After the structural characterizations of MOC-Mn to demonstrate the successful decoration with manganese carbonyl moieties, the light-triggered CO-release behaviour of MOC-Mn was also studied to exhibit a controlled release process. The *in vitro* and *in vivo* biocompatibility of MOC-Mn were evaluated to verify its low toxicity and good biocompatibility, which may contribute to the reduction of metal toxicity from the CO-released manganese residuals which were stabilized within the MOC skeleton in this CORMA. Through light-triggered CO release, MOC-Mn can effectively inhibit the survival of HeLa cells.

2. Results and discussion

2.1 Preparation and characterization of MOC-Mn

Details of the preparation and characterization of MOC and MOC-Mn are described in ESI.† Through static heating at 65 °C in DMSO, H_2BPyDC ligand, and excess zirconocene dichloride (Cp_2ZrCl_2, Cp = η^5-C_5H_5), which was hydrolyzed to 3-connected trinuclear pyramidal Zr_3O clusters ($Zr_3Cp_3O(OH)_3$), were converted to discrete and stable crystalline MOC tetrahedrons (Fig. S1, ESI†).[24] The off-white MOC crystals can be dissolved in DMSO-d_6 to acquire the nuclear magnetic resonance (NMR) spectrum as shown in Fig. 1A and Fig. S2 (ESI†). The characteristic signals and integral areas of the bipyridyl ligands and Cp moieties within the Zr_3O cluster meet well with theoretical positions and values. The observed ESI mass spectra of the MOC (Fig. S3, ESI†) have peaks at *m/z* 1796.7411 and 898.8744, which are the signals from $[M\text{-}4Cl\text{-}2H]^{2+}$ and $[M\text{-}4Cl]^{4+}$ ions, respectively, consistent with the calculated theoretical values and the tested values in a previous report.[25]

Due to the freely accessible bipyridyl sites within the MOC, the inorganic CO-releasing molecules can coordinate with the MOC skeleton to form a CORMA through PSM.[26] The MOC was then decorated with $Mn(CO)_5Br$ in tetrahydrofuran and toluene to obtain MOC-Mn as an orange powder (Fig. S4, ESI†). The ^{1}H-NMR spectrum of MOC-Mn in DMSO-d_6 (Fig. 1A and Fig. S5, ESI†) also exhibited the characteristic signals from the bipyridyl and Cp moieties with obvious peak broadening and shifts. The integral areas of these signals also comply with the corresponding stoichiometric ratios of MOC. The above signals all moved toward higher fields after coordination due to the electronic effect. These broadened signals may have resulted from the uncertain number (*i.e.*, 0–6) of $Mn(CO)_3Br$ moieties within one MOC-Mn and the increased hydrodynamic dimensions. Although the uncertain loading number and complex charge were caused by the instability of carbonyl moieties under the ESI test conditions and the deteriorated solubility of MOC-Mn. The ESI mass spectra (Fig. S6, ESI†) of MOC-Mn with multiple peaks are consistent with MOC-Mn fragments as shown in Table S1 (ESI†). The CO loss may come from the loading process or the ESI testing process. Moreover, compared with the MOC, the FTIR spectra of MOC-Mn (Fig. 1B and Fig. S7, ESI†) present strong bands at 1934 and 2032 cm^{-1} that were assigned to the stretching vibrations of the carbonyl moieties.

The appearance of C, N, O, Zr, and Mn in the X-ray photoelectron spectrum (XPS) further supported the successful loading of $Mn(CO)_3Br$ moieties within the MOC-Mn (Fig. 1C). For the XPS analysis of Mn, as shown in Fig. 1D, two main peaks of $Mn2p_{3/2}$ and $Mn2p_{1/2}$ appeared from 638–663 eV.[27] It has been established in the literature that the binding energy of $Mn(CO)_5Br$ is 642.1 eV, which is reduced to 641.2 eV for $Mn(CO)_3Br[P(OCH_3)_3]_2$ due to the presence of the electronegative group, which weakens the donor ability of the ligand.[28] In this study, the binding energy of Mn2p at $Mn(CO)_3Br$ was reduced to 641.05 eV due to the weakening of the binding energy by the bipyridyl sites within the MOC-Mn. All these structural characterizations verified that $Mn(CO)_3Br$ moieties were successfully coordinated to the MOC skeleton.

The images from scanning electron microscope (SEM) and energy dispersive spectrometer (EDS) elemental mapping of MOC-Mn are shown in Fig. S8 (ESI†) and indicate the partially crystalline structures and uniform elemental distribution of

Mn, Zr, N, *et al.* To quantitatively confirm the loading amount of $Mn(CO)_3Br$ moieties, the MOC-Mn sample was digested to conduct inductively coupled plasma-mass spectroscopy (ICP-MS). The measured ratio of Zr to Mn was close to 2 : 1, indicating that the average loading number of $Mn(CO)_3Br$ moieties is about 6 for each MOC tetrahedron, *i.e.*, there is a high loading efficiency.

2.2 Light-triggered CO release from MOC-Mn

Due to the light instability of most metal-based CO-releasing molecules, the light-triggered release behaviour of MOC-Mn was also estimated. Due to the strong affinity of CO to deoxy-Mb (myoglobin), CO binds to deoxy-Mb to form CO-bound Mb (MbCO). In the UV-vis spectrum, deoxy-Mb has a characteristic absorption peak at 560 nm, while MbCO has peaks at 540 and 578 nm. Taking advantage of this switch in the characteristic absorption peak for the conversion of deoxy-Mb to MbCO, the light-triggered release of CO from MOC-Mn was assessed using a UV-vis spectrophotometer. Under light irradiation at 365 nm (5 W with filter and distance of 10 cm) for different times, it can be seen that the characteristic peak at 560 nm from deoxy-Mb gradually decayed, while the characteristic peaks at 540 and 578 nm from MbCO gradually enhanced as shown in Fig. 2A. In addition, obvious colour changes (Fig. S9, ESI†) and continuous bubbling during the CO release process of MOC-Mn under 365 nm light irradiation (video 1, ESI†) further demonstrated effective release of CO. The process of MOC-Mn light-triggered CO release was monitored by UV-vis spectroscopy every 10 min, and the released CO gradually increased with the irradiation time until there was no significant change in the spectrum, indicating that most of the CO was released after 60 min; this was much slower than Mn-based CORMs.[29] The amount of MbCO generated during this release process was calculated as shown in Fig. 2B.[30] The obtained MOC-Mn is stable enough in the absence of light for over a year due to similar CO-release behaviour for the related sample. The FTIR spectrum of MOC-Mn before and after light irradiation was conducted (Fig. S7, ESI†). Irradiation of MOC-Mn under light induced a gradual weakening of the carbonyl vibrational bands at 1934 and 2032 cm^{-1} with increasing irradiation time, suggesting effective CO release. However, all peaks – other than carbonyl peaks – are preserved after CO release, indicating the structural integrity of the MOC skeleton after CO release. Related works on the photocatalytic studies of such MOCs also indicate structural stability during continuous irradiation under visible light.[31,32]

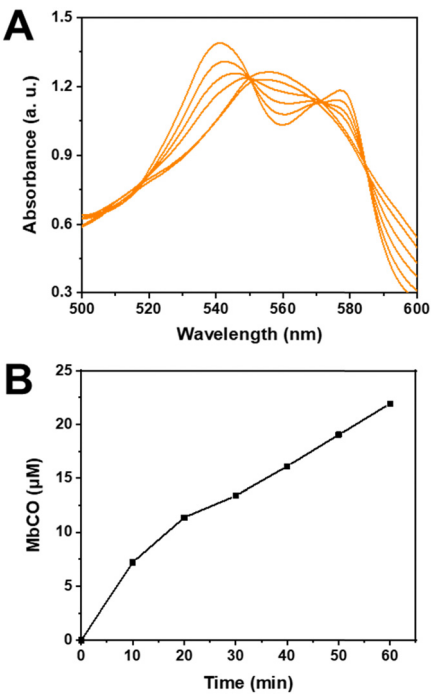

Fig. 2 The CO-release behaviour from MOC-Mn under light irradiation. (A) UV-vis spectra during the CO release. (B) The generation of MbCO over time.

To estimate Mn leakage from MOC-Mn during the light-triggered CO release process, the MOC-Mn after CO release was isolated through centrifugation and analyzed with ICP-MS. The results revealed that less than 10% of the Mn was leaked, indicating that most of the Mn residue was retained on the MOC skeleton, effectively reducing its potential toxicity. Compared to Mn(CO)5Br, the prolonged CO release time and reduced toxicity of MOC-Mn make it an excellent candidate for CORMA.

2.3 Biocompatibility of MOC-Mn

The uptake of MOC-Mn into HeLa cells was evaluated using ICP-MS (Fig. S10, ESI†). After 8 h of cell uptake, the contents of Zr and Mn no longer increased significantly, and the contents of Zr and Mn were close to 2 : 1, which is consistent with the previous ICP-MS results for as-synthesized MOC-Mn. The ICP-MS results indicated the effective uptake of MOC-Mn into HeLa cells. The cytotoxicity of MOC-Mn was determined by hemolytic assay and MTT (3-(4,5-dimethylthiazol-2-yl)-2,5-diphenyltetrazolium bromide) method in the absence of light. Briefly, different concentrations of MOC-Mn solution (ranging from 25 μg mL^{-1} to 800 μg mL^{-1}) were tested in addition to a control comprising double distilled water (DDW). It is found that the hemolysis ratio with different concentrations of MOC-Mn were all lower than 1%, indicating the nontoxic nature of MOC-Mn for erythrocytes as shown in Fig. 3A. In line with the results of the hemolytic assay, MTT also showed excellent biocompatibility of MOC-Mn. As shown in Fig. 3B, the cell viability of HeLa cells was stable at 97% even in the presence of a high concentration of MOC-Mn (800 μg mL^{-1}).

At different time points after caudal vein injection of MOC-Mn solution (800 μg mL^{-1}, 200 μL), blood biochemistry assay of kidney and liver injury biomarkers were carried out, including blood urea nitrogen (BUN), creatinine (CRE), alanine transaminase (ALT), aspartate transaminase (AST), lactate dehydrogenase (LDH), and alkaline phosphatase (ALP). There was a negligible difference in these damage biomarkers among the different groups, indicating the biosafety of MOC-Mn *in vivo*. As observed in hematoxylin and eosin (H&E) staining of harvested kidney, heart, liver, spleen, and lung, there was no apparent toxicity of

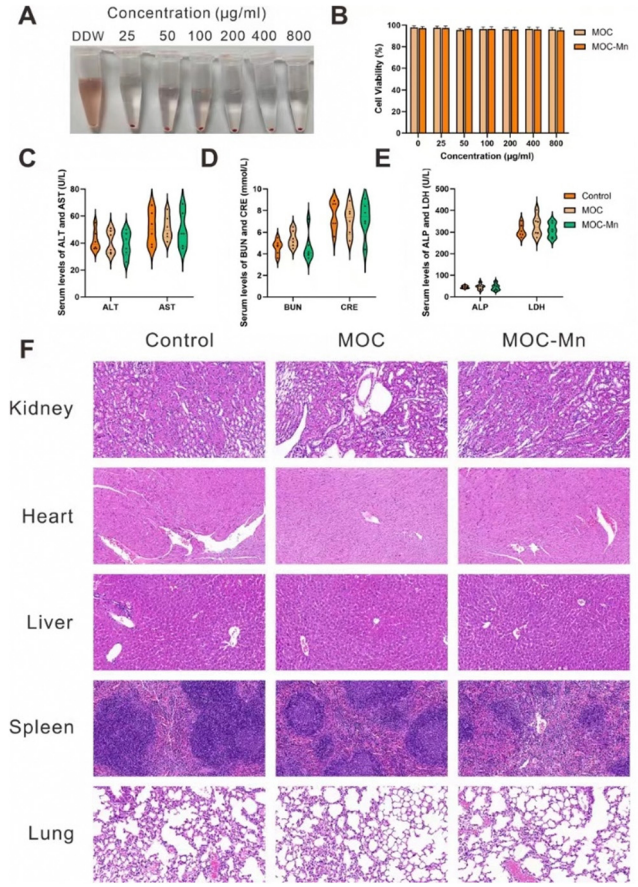

Fig. 3 The biocompatibility of MOC-Mn. (A) The hemolysis test of red blood cells with MOC-Mn in different concentrations. (B) The MTT assay of HeLa cells with MOC or MOC-Mn in different concentrations. (C)–(E) The contents of ALT, AST, BUN, CRE, ALP, and LDH reflect the signs of cell injury before and after the administration of MOC-Mn. (F) H&E staining of kidney, heart, liver, spleen, and lung of mice before and after intravenous injection.

MOC-Mn on these major organs. These results together demonstrate that MOC-Mn exhibits high biocompatibility, and thus, has potential medical use. The good biocompatibility of MOC-Mn may contribute to the reduction of metal toxicity from the CO-released manganese residuals which were stabilized within the MOC skeleton.

2.4 Biological assays

MTT cytotoxicity analysis of HeLa cells treated with different concentrations of MOC-Mn under light irradiation (365 nm) was conducted. As shown in Fig. 4, MOC-Mn can effectively inhibit the survival of HeLa cells. As the content of MOC-Mn increased, the survival of HeLa cells decreased with IC_{50} of $\sim$15 μg mL^{-1}.

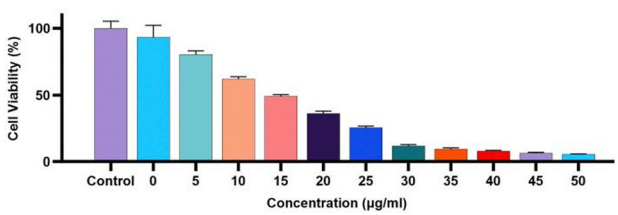

Fig. 4 MTT analysis of MOC-Mn on HeLa cells under light irradiation.

3. Conclusions

An atomically precise nanocarrier, MOC, was introduced to bond CO-releasing molecules effectively to form a new type of CORMA. This MOC-based CORMA showed light-controlled CO release under irradiation of light. The effective preparation of the MOC-based CORMA and the light-controlled CO release was confirmed by NMR, FTIR, XPS, SEM, ICP-MS, and UV-vis analyses, revealing the possibility of exogenous CO delivery to the therapeutic location. According to the hemolysis test, MTT test, and H&E staining of mouse organs, this MOC-based CORMA exhibits low toxicity and good biocompatibility both *in vitro* and *in vivo*. The MTT assay of HeLa cells illustrated good tumor cell inhibition through light-triggered CO release from MOC-Mn. The proposed well-defined nanoscale CORMA is beneficial for studying structure–activity relationships, which can optimize clinical performances and increase the potentiality for clinical transformation.

Author contributions

Y. W. and J. Y. designed the study, the main conceptual ideas, and the proof outline. X. N., P. Y. and J. Y. ran the experiments and collected the data. X. N., Y. W., and J. Y. wrote the manuscript. F. G. supervised the project. All authors discussed the results and commented on the manuscript.

Conflicts of interest

There are no conflicts to declare.

Acknowledgements

This work was supported by the National Key R&D Program of China (Key Special Project for Marine Environmental Security and Sustainable Development of Coral Reefs 2022–3.5), the Fundamental Research Funds for the Central Universities (YG2023QNA04, YG2022QN027), and Shanghai Municipal Health Commission Clinical Research Project (20214Y0521).

Notes and references

1 S. H. Heinemann, T. Hoshi, M. Westerhausen and A. Schiller, *Chem. Commun.*, 2014, **50**, 3644–3660.
2 D. Morse, J. Sethi and A. M. Choi, *Crit. Care Med.*, 2002, **30**, S12–17.
3 K. Ling, F. Men, W. C. Wang, Y. Q. Zhou, H. W. Zhang and D. W. Ye, *J. Med. Chem.*, 2018, **61**, 2611–2635.
4 S. W. Ryter and A. M. Choi, *Curr. Opin. Pharmacol.*, 2006, **6**, 257–262.

5 T. Slanina and P. Šebej, *Photochem. Photobiol. Sci.*, 2018, **17**, 692–710.
6 H. I. Choi, A. Zeb, M. S. Kim, I. Rana, N. Khan, O. S. Qureshi, C. W. Lim, J. S. Park, Z. Gao, H. J. Maeng and J. K. Kim, *J. Controlled Release*, 2022, **350**, 652–667.
7 K. Fujita, Y. Tanaka, S. Abe and T. Ueno, *Angew. Chem., Int. Ed.*, 2016, **55**, 1056–1060.
8 H. Meyer, F. Winkler, P. Kunz, A. M. Schmidt, A. Hamacher, M. U. Kassack and C. Janiak, *Inorg. Chem.*, 2015, **54**, 11236–11246.
9 M. Ma, H. Noei, B. Mienert, J. Niesel, E. Bill, M. Muhler, R. A. Fischer, Y. Wang, U. Schatzschneider and N. Metzler-Nolte, *Chemistry*, 2013, **19**, 6785–6790.
10 F. J. Carmona, S. Rojas, P. Sánchez, H. Jeremias, A. R. Marques, C. C. Romão, D. Choquesillo-Lazarte, J. A. Navarro, C. R. Maldonado and E. Barea, *Inorg. Chem.*, 2016, **55**, 6525–6531.
11 C. Liu, Z. Du, M. Ma, Y. Sun, J. Ren and X. Qu, *iScience*, 2020, **23**, 101483.
12 Y. Li, Z. Liu, W. Zeng, Z. Wang, C. Liu, N. Zeng, K. Zhong, D. Jiang and Y. Wu, *Front. Oncol.*, 2021, **11**, 738567.
13 S. Diring, A. Carné-Sánchez, J. Zhang, S. Ikemura, C. Kim, H. Inaba, S. Kitagawa and S. Furukawa, *Chem. Sci.*, 2017, **8**, 2381–2386.
14 H. Meyer, M. Brenner, S. P. Höfert, T. O. Knedel, P. C. Kunz, A. M. Schmidt, A. Hamacher, M. U. Kassack and C. Janiak, *Dalton Trans.*, 2016, **45**, 7605–7615.
15 Q. Dai, L. Wang, E. Ren, H. Chen, X. Gao, H. Cheng, Y. An, C. Chu and G. Liu, *Angew. Chem., Int. Ed.*, 2022, **61**, e202211674.
16 X. Ning, X. Zhu, Y. Wang and J. Yang, *Bioact. Mater.*, 2024, **37**, 30–50.
17 C. Yu, P. Yang, X. Zhu and Y. Wang, *Sci. China: Chem.*, 2022, **65**, 858–862.
18 S. Lee, H. Jeong, D. Nam, M. S. Lah and W. Choe, *Chem. Soc. Rev.*, 2021, **50**, 528–555.
19 S. Y. Yin, Y. X. Zhu, M. Pan, Z. W. Wei, H. P. Wang, Y. N. Fan and C. Y. Su, *Eur. J. Inorg. Chem.*, 2017, 646–650.
20 H. J. Yu, Z. M. Liu, M. Pan, K. Wu, Z. W. Wei, Y. W. Xu, Y. N. Fan, H. P. Wang and C. Y. Su, *Eur. J. Inorg. Chem.*, 2018, 80–85.
21 G. Liu, M. Zeller, K. Su, J. Pang, Z. Ju, D. Yuan and M. Hong, *Chemistry*, 2016, **22**, 17345–17350.
22 G. Liu, Z. Ju, D. Yuan and M. Hong, *Inorg. Chem.*, 2013, **52**, 13815–13817.
23 D. Sun, X. Feng, X. Zhu, Y. Wang and J. Yang, *Coord. Chem. Rev.*, 2024, **500**, 215546.
24 E.-S. M. El-Sayed, Y. D. Yuan, D. Zhao and D. Yuan, *Acc. Chem. Res.*, 2022, **55**, 1546–1560.
25 N. Xu, Y. Tan, E. El-Sayed and D. Yuan, *Cryst. Growth Des.*, 2022, **22**, 2768–2773.
26 J. Liu, Z. Wang, P. Cheng, M. J. Zaworotko, Y. Chen and Z. Zhang, *Nat. Rev. Chem.*, 2022, **6**, 339–356.
27 B. Thirupathi and P. G. Smirniotis, *Appl. Catal., B*, 2011, **110**, 195–206.
28 L. F. Wuyts, D. F. Van de Vondel, G. P. Van der Kelen and L. Bevernage, *J. Electron Spectrosc. Relat. Phenom.*, 1977, **10**, 389–392.
29 M. Hu, Y. Yan, B. Zhu, F. Chang, S. Yu and G. Alatan, *RSC Adv.*, 2019, **9**, 20505–20512.
30 A. J. Atkin, J. M. Lynam, B. E. Moulton, P. Sawle, R. Motterlini, N. M. Boyle, M. T. Pryce and I. J. Fairlamb, *Dalton Trans.*, 2011, **40**, 5755–5761.
31 C. Ji, W. Wang, E.-S. M. El-Sayed, E.-S. M. El-Sayed, G. Liu, Y. Si, K. Su, Z. Ju, F. Wu and D. Yuan, *Appl. Catal., B*, 2021, **285**, 119782.
32 X.-J. Qi, R.-L. Zhong, M. Chen, C. Sun, S.-Q. You, J. Gu, G. Shan, D.-X. Cui, X. Wang and Z. Su, *ACS Catal.*, 2021, **11**, 7241–7248.